Crystal Structures of the G Protein $G_{i\alpha1}$ Complexed with GDP and Mg^{2+}: A Crystallographic Titration Experiment‡

David E. Coleman§ and Stephen R. Sprang*,§,||

Howard Hughes Medical Institute and Department of Biochemistry, The University of Texas Southwestern Medical Center, 5323 Harry Hines Boulevard, Dallas, Texas 75235-9050

Received May 5, 1998; Revised Manuscript Received August 10, 1998

ABSTRACT: The effect of Mg^{2+} binding on the conformation of the inactive GDP-bound complex of the heterotrimeric G protein α subunit $G_{i\alpha1}$ has been investigated by X-ray crystallography. Crystal structures of the $G_{i\alpha1}$·GDP complex were determined after titration with 5, 10, 100, and 200 mM Mg^{2+}. Comparison of these structures with that of the Mg^{2+}-free complex revealed Mg^{2+} bound at the same site as observed in the structure of the active, $G_{i\alpha1}$·GTPγS·Mg^{2+}-bound complex of $G_{i\alpha1}$, with a similar coordination scheme except for the substitution of a water molecule for an oxygen ligand of the γ-phosphate of $G_{i\alpha1}$·GTPγS·Mg^{2+}. In contrast to the GDP·Mg^{2+} complex of $G_{t\alpha}$ and of other G proteins, switch I residues of $G_{i\alpha1}$ participate in Mg^{2+} binding and undergo conformational changes as a consequence of Mg^{2+} binding. Partial order is induced in switch II, which is disordered in the Mg^{2+}-free complex, but no order is observed in the switch III region. This contrasts with the GDP·Mg^{2+} complex of $G_{t\alpha}$ in which both switch II and III switch are ordered. Mg^{2+} binding also induces binding of an SO_4^{2-} molecule to the active site in a manner which may mimic a $G_{i\alpha1}$·GDP·PO_4^{2-}·Mg^{2+} product complex. Implications of these findings are discussed.

The α subunits of heterotrimeric G proteins (G_α) are GTPases which, in concert with G protein heterodimers composed of β and γ subunits ($G_{\beta\gamma}$), transduce intracellular signals from membrane-bound receptors to downstream effector molecules (*1*, *2*). Biological activities which employ $G_{\alpha\beta\gamma}$ proteins include vision, hormone-mediated responses, and synaptic nerve signal transmission. $G_{\alpha\beta\gamma}$ proteins couple activated membrane-bound receptors to downstream effector molecules by cycling between inactive (nonsignaling) and active (signaling) states. In the inactive state, $G_{\alpha\beta\gamma}$ proteins exist as heterotrimeric $G_{\alpha\beta\gamma}$·GDP complexes with GDP bound tightly to the G_α subunit. Upstream signaling events begin when ligand-activated receptors catalyze the exchange of GDP bound to the G_α subunit for GTP·Mg^{2+}. Binding of GTP·Mg^{2+} to the G_α subunit results in dissociation of the heterotrimer, forming free $G_{\beta\gamma}$ complex and the active, G_α·GTP·Mg^{2+} species. $G_{\beta\gamma}$ and the active G_α·GTP·Mg^{2+} complex may then bind to and regulate downstream effectors. Upon hydrolysis of G_α·GTP·Mg^{2+} to G_α·GDP by the GTPase activity of G_α [in some cases assisted by stimulatory proteins (*3*, *4*)], the inactive G_α·GDP complex dissociates from effector and combines with $G_{\beta\gamma}$ to re-form the nonsignaling $G_{\alpha\beta\gamma}$·GDP complex. The $G_{\alpha\beta\gamma}$·GDP complex may then rebind to receptor and undergo further rounds of the signal transduction cycle.

G_α subunits belong to the G protein superfamily of GTPases, members of which contain a conserved guanine nucleotide binding domain and cycle between inactive GDP-bound and active GTP-bound states (*5*, *6*). $G_{i\alpha1}$, the subject of this report, is activated by α2-adrenergic (*7*) and m2 muscarinic receptors (*8*) and inhibits isoforms I, V, and VI of adenylyl cyclase (*9*, *10*).

The conformational changes that occur within G proteins have been observed by X-ray crystallographic analysis of G proteins activated with either GDP or nonhydrolyzable GTP analogues and Mg^{2+}. Comparison of the active and inactive structures of Ras (*11*−*13*) and other G proteins (*14*, *15*) has revealed two polypeptide segments that differ significantly in conformation in the GDP- and GTP-bound states. These two regions, dubbed switch I and switch II, contribute residues that are involved in binding the γ-phosphate of GTP and Mg^{2+} (e.g., Figure 1). Structures of G proteins complexed with effectors (*16*, *17*) or other proteins (*18*, *19*) reveal that switch I and switch II are also involved in nucleotide-dependent protein−protein interactions. In particular, the structure of $G_{s\alpha}$ complexed with the catalytic domain of its effector, adenylyl cyclase, indicates that switch II directly interacts with the effector (*17*). Switch I and II thus constitute the heart of the conformational switching mechanism which both senses the presence or absence of a γ-phosphate group within the active site and controls the interaction of G proteins with other molecules.

Crystallographic determinations of the active and inactive structures of the heterotrimeric G protein α subunits transducin ($G_{t\alpha}$) and $G_{i\alpha1}$ have revealed the conformational changes that switch I and switch II undergo, and have identified an additional conformationally active region, switch III (*20*−*23*). Curiously, although the switch regions

‡ X-ray coordinates for the $G_{i\alpha1}$·GDP·Mg^{2+} complex have been deposited in the Brookhaven Protein Data Bank under the file name 1bof.

* Address correspondence to this author at the Howard Hughes Medical Institute, The University of Texas Southwestern Medical Center at Dallas, 5323 Harry Hines Blvd., Dallas, TX 75235-9050. E-mail: Sprang@howie.swmed.edu. Phone: 214 648-5008. Fax: 214 648-6336.

§ Department of Biochemistry.

|| Howard Hughes Medical Institute.

S0006-2960(98)01030-7 CCC: $15.00 © 1998 American Chemical Society
Published on Web 09/15/1998

and other features of $G_{t\alpha}$ and $G_{i\alpha1}$ are essentially identical in the active GTPS·Mg^{2+}-bound[1] complexes, the inactive, GDP-bound complexes are distinctly different. In particular, switch II and switch III are completely disordered in $G_{i\alpha1}$·GDP whereas they are well-ordered in $G_{t\alpha}$·GDP. The dissimilarity between these inactive, GDP-bound structures implies that their mechanism of dissociation from their respective effectors may also differ. Alternatively, a possible reason for these differences is that $G_{t\alpha}$·GDP (crystallized in 200 mM Mg^{2+}) has Mg^{2+} bound to the active site, whereas $G_{i\alpha1}$·GDP (crystallized in the absence of Mg^{2+}) does not.

G proteins are sensitive to the presence or absence of Mg^{2+}. All members of the G protein family require Mg^{2+} in order to catalyze hydrolysis of GTP (*1*, *24*). Structures of G proteins complexed with nonhydrolyzable GTP analogues and Mg^{2+} (including $G_{t\alpha}$ and $G_{i\alpha1}$) show that Mg^{2+} binds to the active site and interacts with switch I, and the β/γ-phosphate groups (*14*, *15*). Similarly, structures of G proteins complexed with GDP and Mg^{2+} reveal Mg^{2+} bound to the same position; however, the conformation of switch I is altered such that it is no longer involved in Mg^{2+} binding.

Many nonheterotrimeric G proteins, such as EF-Tu and Ras, bind Mg^{2+} in the GDP-bound state, with Mg^{2+} increasing their affinity for GDP (*25*−*27* and references cited therein). It has been proposed that some nucleotide exchange mechanisms release GDP, in part, by disrupting Mg^{2+} binding (*28*−*30*), and that physiologically Mg^{2+} may maintain the inactive state by acting as a nucleotide dissociation inhibitor (*27*). This activity would prevent nucleotide exchange—and hence unwarranted activation by GTP—in the absence of a nucleotide exchange factor (*27*). For these proteins, the transition between the active and the inactive state is mediated by the presence or absence of the γ-phosphate group of GTP alone.

In contrast, Mg^{2+} binds to heterotrimeric G protein G_{α}·GDP and $G_{\alpha\beta\gamma}$·GDP complexes with weak affinity, does not increase GDP binding affinity, and is not required in order to maintain the inactive, GDP-bound state (*31*). However, as noted, the structure of the GDP-bound complex of the heterotrimeric G protein α subunit transducin ($G_{t\alpha}$) (crystallized in 200 mM Mg^{2+}) (*21*) reveals Mg^{2+} bound to the active site in a manner that is similar to that observed in other G protein GDP·Mg^{2+} complexes. This finding indicates that, in at least one case, Mg^{2+} can bind to a G_{α}·GDP complex, although it is not known whether Mg^{2+} binds to this complex at physiological concentrations of Mg^{2+}. In contrast, the structure of the GDP-bound complex of the homologous heterotrimeric G protein α subunit $G_{i\alpha1}$ (crystallized in the absence of Mg^{2+}) exhibits an empty Mg^{2+} binding site, and is thus a rare example of a GDP-bound G protein structure which contains no Mg^{2+} and is not complexed with other proteins (*23*). [The structure of the EF-G·GDP complex also contains no Mg^{2+}; this molecule does not bind GDP well, and appears to undergo nucleotide exchange without the need for an exchange factor (*32*).]

The lack of order of switch II and III in $G_{i\alpha1}$·GDP, in contrast to $G_{t\alpha}$·GDP·Mg^{2+}, could be a consequence of the absence of Mg^{2+} in the $G_{i\alpha1}$·GDP complex. It is possible that, like $G_{t\alpha}$, Mg^{2+} may bind to $G_{i\alpha1}$·GDP and might then stabilize these regions, providing an alternate model of the inactive state. Alternatively, failure of Mg^{2+} to induce order in these regions would strengthen, in the case of $G_{i\alpha1}$, the hypothesis that these regions become completely disordered after loss of the γ-phosphate group of GTP and that this loss of order promotes dissociation from effector.

The possibility that Mg^{2+} binding may induce conformational changes in $G_{i\alpha1}$·GDP may also reveal some of the effects of Mg^{2+} during activation of $G_{i\alpha1}$. Full activation of G proteins following exchange of GDP for GTP appears to require Mg^{2+} bound to the active site. Conformational changes upon addition of Mg^{2+} to isolated G_{α}·GTP subunits can be observed by changes in fluorescence intensity (*33*, *34*) and decreased sensitivity to trypsin digestion (*35*, *36*). G_{α} subunits bearing certain mutations ($G_{s\alpha}$: G226A, $G_{i\alpha1}$: G203A or G42V) behave normally as isolated α subunits (that is, they bind GTP and have normal GTPase activity and unaltered ability to modulate effectors), but have lost the ability to dissociate from the $G_{\alpha\beta\gamma}$·GTP complex (*37*−*39*). These mutant G_{α} subunits have greatly reduced affinity for Mg^{2+} and appear to have lost the ability to adopt the fully active conformation. It is inferred from these observations that Mg^{2+} must bind to the $G_{\alpha\beta\gamma}$·GTP complex in order to effect release of G_{α}·GTP from the heterotrimer. Magnesium ion may thus play a structural role in the mechanism of conformational switching to the active G_{α}·GTP·Mg^{2+} state in addition to its role in catalysis.

To determine whether Mg^{2+} can bind to crystalline G_{α}·GDP complexes, to elucidate its mode of binding, and to investigate its potential role in conformational changes, we have solved a series of structures of $G_{i\alpha1}$·GDP complexed with Mg^{2+}. The experiment was carried out as an X-ray crystallographic titration experiment in which crystals of the $G_{i\alpha1}$·GDP complex containing 5, 10, 100, and 200 mM Mg^{2+} were chosen for structure determination in order to map out the lower and upper limits of potential Mg^{2+} effects. These structures have been compared to the structures of the Mg^{2+}-free $G_{i\alpha1}$·GDP complex, the $G_{i\alpha1}$·GTPγS·Mg^{2+} and $G_{t\alpha}$·GTPγS·Mg^{2+} complexes, and other G protein structures. The titrated structures reveal that Mg^{2+} does bind to $G_{i\alpha1}$·GDP but that the mode of binding differs from that observed in other G protein GDP·Mg^{2+}-bound complexes. Conformational changes in switch I and limited ordering of switch II are observed; however, switch II and switch III remain essentially disordered. In addition, Mg^{2+} promotes binding of SO_4^{2-} to the active site, thus forming a $G_{i\alpha1}$·GDP·Mg^{2+}·SO_4^{2-} complex which may mimic a $G_{i\alpha1}$·GDP·Mg^{2+}·PO_4^{2-} ternary product complex formed following GTP hydrolysis. Implications of these effects with respect to Mg^{2+}-induced changes during activation, events following hydrolysis of GTP, and loss of effector binding affinity are discussed.

EXPERIMENTAL PROCEDURES

Crystallization and Data Collection. Nonmyristoylated, nonpalmitoylated recombinant rat $G_{i\alpha1}$ (354 residues, 40.5 kDa) was synthesized in *E. coli* and purified as described previously (*40*). Crystals of $G_{i\alpha1}$·GDP·Mg^{2+} were grown in ammonium sulfite under conditions identical to those used to obtain crystals of the Mg^{2+}-free $G_{i\alpha1}$·GDP complex (*41*), except that either 5 or 10 mM $MgSO_4$ was included in the crystallization solution. Crystals do not grow in solutions

[1] Abbreviations: DTT, dithiothreitol; EDTA, ethylenediaminetetraacetic acid; GTPγS, guanosine 5′-*O*-3-thiotriphosphate.

Table 1: Data Collection Statistics

data set[a]	X-ray source	total obsd	unique obsd	resolution (Å)	completeness (%)	R_{merge}[b]	$\langle I/\sigma \rangle$
5 mM Mg^{2+}	RaxisII	74197	15461	15−2.6	99.8	0.080	20.4
10 mM Mg^{2+}	CHESS[c] A1	74642	22913	15−2.2	89.7	0.052	18.9
100 mM Mg^{2+}	RaxisII	65673	15379	15−2.6	99.5	0.080	17.2
200 mM Mg^{2+}	CHESS A1	91667	25367	15−2.2	97.3	0.039	27.5

[a] All data sets collected at 100 K. [b] $R_{merge} = 100 \times \sum|I_{hkl} - \langle I_{hkl}\rangle|/\sum\langle I_{hkl}\rangle$. [c] CHESS: Cornell High Energy Synchrotron Source.

Table 2: Refinement Statistics

data set	protein atoms	solvent atoms	resolution (Å)	R[a] (%)	R_{free}[b] (%)
5 mM Mg^{2+}	2583	51	15−2.6	21.4	25.9
10 mM Mg^{2+}	2583	83	15−2.2	21.8	26.6
100 mM Mg^{2+}	2591	60	15−2.6	21.5	25.5
200 mM Mg^{2+}	2591	88	15−2.2	23.0	26.7

[a] $R = 100 \times \sum||F_o| - |F_c||/\sum|F_o|$. [b] $R_{free} = R$ for a random 10% of the data excluded from the refinement.

containing [$MgSO_4$] above 10 mM. Therefore, crystals containing 100 or 200 mM Mg^{2+} were prepared by transferring crystals grown in 10 mM $MgSO_4$ into Li_2SO_4 stabilization solutions containing 100 or 200 mM $MgSO_4$ as described below. Crystals containing Mg^{2+} are isomorphous to Mg^{2+}-free crystals and belong to space group *I4* with $a, b = 121.3$ Å and $c = 67.7$ Å, and contain one molecule per asymmetric unit. Crystals were prepared for freezing by first stabilizing them in a solution containing 2.0 M Li_2SO_4, 1 mM GDP, 3 mM DTT, 100 mM *N*,*N*-bis(2-hydroxyethyl)-2-aminoethanesulfonic acid (BES) (pH 7.0), and either 5, 10, 100, or 200 mM $MgSO_4$. The crystals were then sequentially transferred into the above solution containing 5%, 10%, 15%, and finally 20% glycerol (v/v) included as a cyroprotectant. Approximately 15 min passed between each transfer step. Crystals were flash-frozen on rayon loops by plunging them into either liquid nitrogen (5, 10, and 100 mM Mg^{2+} crystals) or liquid propane (200 mM Mg^{2+} crystals), and stored in liquid nitrogen prior to data collection. These stabilization and freezing conditions are identical to those used previously for the Mg^{2+}-free $G_{i\alpha1}$·GDP crystals (*23*), except for the inclusion of Mg^{2+} and the absence of EDTA. X-ray diffraction data were collected using either a Rigaku RU300 rotating anode generator equipped with an Raxis II phosphor-imaging plate detector or the Cornell synchrotron source (CHESS) A1 line ($\lambda = 0.91$ Å) equipped with a CCD detector (Table 1). Data were processed using the DENZO/SCALEPACK programming package (*42*). A Wilson scaling procedure implemented using the TRUNCATE feature of the CCP4 protein crystallographic package (*43*) was used to place all data on an approximate absolute scale to facilitate map comparisons. Data set collection statistics are given in Table 1.

Model Building and Refinement. Initial model building was begun using synchrotron data obtained from crystals of $G_{i\alpha1}$·GDP·$Mg^{2+}{}_{10mM}$ as these crystals produced the highest resolution data set before data obtained from $G_{i\alpha1}$·GDP·$Mg^{2+}{}_{200mM}$ crystals became available. The Mg^{2+}-free structure of $G_{i\alpha1}$·GDP (*23*) with the water molecules omitted was used as the starting model. This model was fit to the $G_{i\alpha1}$·GDP·$Mg^{2+}{}_{10mM}$ data by rigid-body refinement using XPLOR (*44*), and was then used to calculate phases for initial maps. Regions of $G_{i\alpha1}$·GDP·$Mg^{2+}{}_{10mM}$ that differed from the $G_{i\alpha1}$·GDP model, and the Mg^{2+} and an SO_4^{2-} bound at the active site, were identified as difference peaks observed in sigmaA-weighted $2F_o - F_c$ and $F_o - F_c$ difference maps (*45*). Simulated annealing omit maps (*46*) were used to confirm that the observed differences were not caused by model bias. The protein model was then manually rebuilt, and the Mg^{2+} and SO_4^{2-} ligands were added using the interactive graphics model building program O (*47*, *48*). Positional and atomic temperature factor refinement was carried out on the rebuilt model using XPLOR (*44*) followed by additional rounds of model building and refinement. In the final rounds, water molecules were added to the model and a bulk solvent correction (*49*) was applied using XPLOR. The free-*R* factor method was used to monitor the refinement (*50*). (In order that the free-*R* factor would not be biased by data used for refinement of the Mg^{2+}-free model, the free-*R* factors for all data sets were calculated using the same reflections chosen for free-*R* factor analysis in the Mg^{2+}-free data set.) The $G_{i\alpha1}$·GDP·Mg_{5mM}, $G_{i\alpha1}$·GDP·Mg_{100mM}, and $G_{i\alpha1}$·GDP·Mg_{200mM} models were built using the above procedure with the $G_{i\alpha1}$·GDP·Mg_{10mM} coordinates as the starting model. In all cases, initial sigmaA-weighted difference maps were made using the Mg^{2+}-free model, and simulated annealing omit maps were used to verify the differences between the $G_{i\alpha1}$·GDP and $G_{i\alpha1}$·GDP·Mg^{2+} structures. Each structure exhibits good stereochemistry, with 90−92% of the residues in the most favored region of the Ramachandran plot as analyzed by PROCHECK (*51*). Model comparisons and superpositions were carried out using O. Final refinement statistics calculated using all data are given in Table 2.

Determination of the Occupancy of the Mg^{2+} and SO_4^{2-} Sites. The occupancies of the Mg^{2+} and SO_4^{2-} sites within the active site of the different crystal structures were estimated using electron difference density maps. Data from each of the Mg^{2+}-titrated crystals were placed on the same scale by individually scaling each set to the Mg^{2+}-free data set using the SCALEIT procedure of the CCP4 package. Prior to scaling, the Mg^{2+}-free data were placed on an approximate absolute scale using the Wilson scaling procedure of the TRUNCATE feature of the CCP4 package. NonsigmaA-weighted $F_o - F_c$ omit maps were then made using coefficients and phases calculated using the scaled data and a model in which the active site Mg^{2+} and SO_4^{2-} were omitted. All maps were calculated using data sets which contain the same number of reflections within 2%, and were calculated for the same resolution range (15−2.6 Å). As a test of the method, Ala 41 was also omitted from the

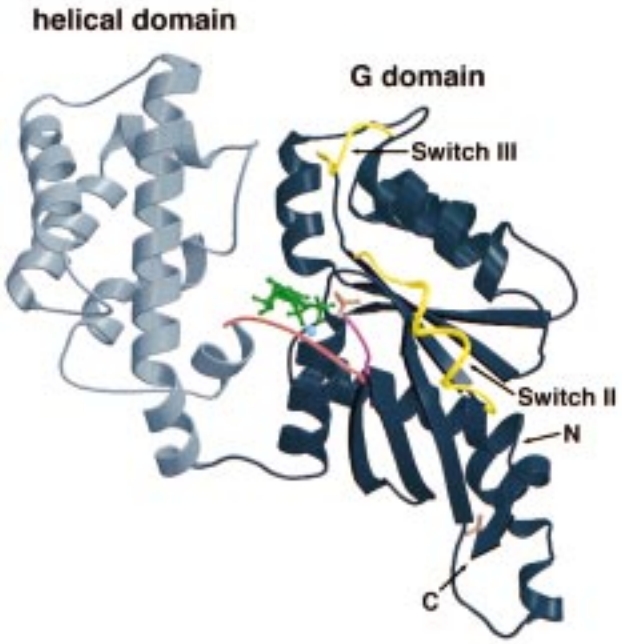

FIGURE 1: Structure of the $G_{i\alpha1}$·GDP·Mg^{2+}·SO_4^{2-} complex in the presence of 200 mM Mg^{2+}. The α-helical and G domains are colored light and dark gray, respectively. N and C indicate the positions of the first ordered residue at the amino terminus (Asp^{10}) and the carboxyl terminus (Leu^{354}). GDP (green), Mg^{2+} (blue), and the two SO_4^{2-} ligands (tan) are shown as ball-and-stick models. Switch I residues (177−185) are colored brown, and the ordered residues of switch I (200−203) are colored magenta. Most of switch II (residues 204−217) and switch III (residues 233−239) are disordered; their conformations as observed in the $G_{i\alpha1}$·GTPγS·Mg^{2+} structure are indicated in yellow. The figure was generated using the program MOLSCRIPT (*60*) and rendered with RASTER3D (*61*).

calculation of the phases and amplitudes. The similar magnitude of the maxima of the difference densities for this residue indicates that the maps are on approximately the same scale. The peak heights observed at the positions of the magnesium and sulfur atoms were then used as estimates of the site occupancies.

RESULTS

Overall Architecture. With the exception of the presence of Mg^{2+} and SO_4^{2-} bound at the active site and the changes in switch I (residues 177−187) and switch II (residues 199−219) (see below), the four $G_{i\alpha1}$·GDP·Mg^{2+} crystal structures are essentially identical to that of $G_{i\alpha1}$·GDP (*23*), with RMS (root-mean-square) differences between the corresponding Cα atoms of 0.18 Å (5 mM Mg^{2+}), 0.21 Å (10 mM Mg^{2+}), and 0.28 Å (100 and 200 mM Mg^{2+}). The overall structure of $G_{i\alpha1}$ (Figure 1) is composed of two domains: a G domain (residues 34−62 and 177−343) which is similar in overall structure to that of Ras (*12*, *13*) and of the corresponding G domains in other members of the G protein family (*14*, *15*); and, inserted into it, a 114 residue α-helical domain (residues 63−176) that is unique to the G_α family. The guanine nucleotide binds to a pocket between the G domain and the helical domain, making direct interactions with the G domain only. This two-domain structure is essentially identical to that of the homologous G protein α-transducin ($G_{t\alpha}$) (*21*) and is similar to that of $G_{s\alpha}$ (*52*). As in the $G_{i\alpha1}$·GDP structure, most of the residues of switch II and switch III (residues 231−242) are disordered, in contrast to their ordered state in the $G_{i\alpha1}$·GTPγS·Mg^{2+} complex. However, certain key residues of switch II (Gly 202−Gly 203) are ordered in the 100 and 200 mM $G_{i\alpha1}$·GDP·Mg^{2+} structures as is discussed below. The $G_{i\alpha1}$·GDP and $G_{i\alpha1}$·GDP·Mg^{2+} structures also possess an additional helical microdomain that is formed by the amino and carboxyl termini (residues 10−33 and 344−354; residues 1−9 are disordered), and which contains an SO_4^{2-} molecule derived from the crystal stabilization solution. The role of this microdomain in α subunit/α subunit interactions has been previously discussed (*23*).

Occupancy and Coordination of Mg^{2+}. Mg^{2+} was observed bound at the active site in each of the four titrated structures. Simulated annealing omit difference density maps computed for each of the four $G_{i\alpha1}$·GDP·Mg^{2+} structures (Figure 2B−F) exhibit electron density at the Mg^{2+} binding site as observed in the structure of the $G_{i\alpha1}$·GTPγS·Mg^{2+} complex (*22*) and the corresponding region of other G proteins (*14*, *15*). This region is devoid of density in the Mg^{2+}-free $G_{i\alpha1}$·GDP complex (Figure 2A). The assignment of this density to Mg^{2+} was based on the correlation between its magnitude and [Mg^{2+}], the location of the density at the previously established Mg^{2+} binding site in $G_{i\alpha1}$·GTPγS·Mg^{2+} and in other G proteins, and the nature of the surrounding ligands. Visual inspection of difference electron density maps and comparison with the same region in the $G_{i\alpha1}$·GDP and $G_{i\alpha1}$·GTPγS·Mg^{2+} structures indicate that occupancy of the site is partial at 5 and 10 mM Mg^{2+}, but approaches that of the $G_{i\alpha1}$·GTPγS·Mg^{2+} structure at 100 and 200 mM Mg^{2+} (Figure 2). The occupancy of this site was roughly estimated using $F_o - F_c$ electron difference density maps in which Mg^{2+} was omitted from the model (Figure 3). These indicate that the Mg^{2+} site is 50% occupied at 5 mM Mg, is 70% occupied at 10 mM Mg^{2+}, and is fully occupied at 100 and 200 mM Mg^{2+}. The equivalent occupancies of the Mg^{2+} site in the 100 and 200 mM Mg^{2+} structures and the absence of significant structural differences between them indicate that the titration of the crystals has reached an end point and that the Mg^{2+} binding site is saturated at 100 mM.

The mode of binding of Mg^{2+} to the $G_{i\alpha1}$·GDP complexes is unlike that observed in other G protein/GDP·Mg^{2+} complexes—it closely resembles the binding of Mg^{2+} to the active $G_{i\alpha1}$·GTPγS·Mg^{2+} complex rather than that observed in the inactive complexes. In the 200 mM Mg^{2+} structure, the inner Mg^{2+} coordination sphere contains six ligands and exhibits octahedral geometry (Figures 4 and 5a). The Mg^{2+} ligands are identical to those that coordinate Mg^{2+} in the $G_{i\alpha1}$·GTPγS·Mg^{2+} structure, except that a water molecule fills the position that is occupied by an oxygen of the γ-phosphate group (Figure 5). The four equatorial ligands are provided by the side chain hydroxyl groups of Ser 47 and Thr 181 (part of switch I), an oxygen from the β-phosphate group of GDP, and a water molecule (water 803). The electron density for water 803 is weak in the 200 mM Mg^{2+} $G_{i\alpha1}$·GDP·Mg^{2+} structure, appearing in difference maps only at low contour levels (Figure 2F), and is not observed in the 5, 10, and 100 mM Mg^{2+} structures (Figure 2B−D), indicating that this site is weakly occupied. Residues corresponding to Ser 47 and Thr 181 are conserved in all members of the G protein family (*5*). In particular, Ser

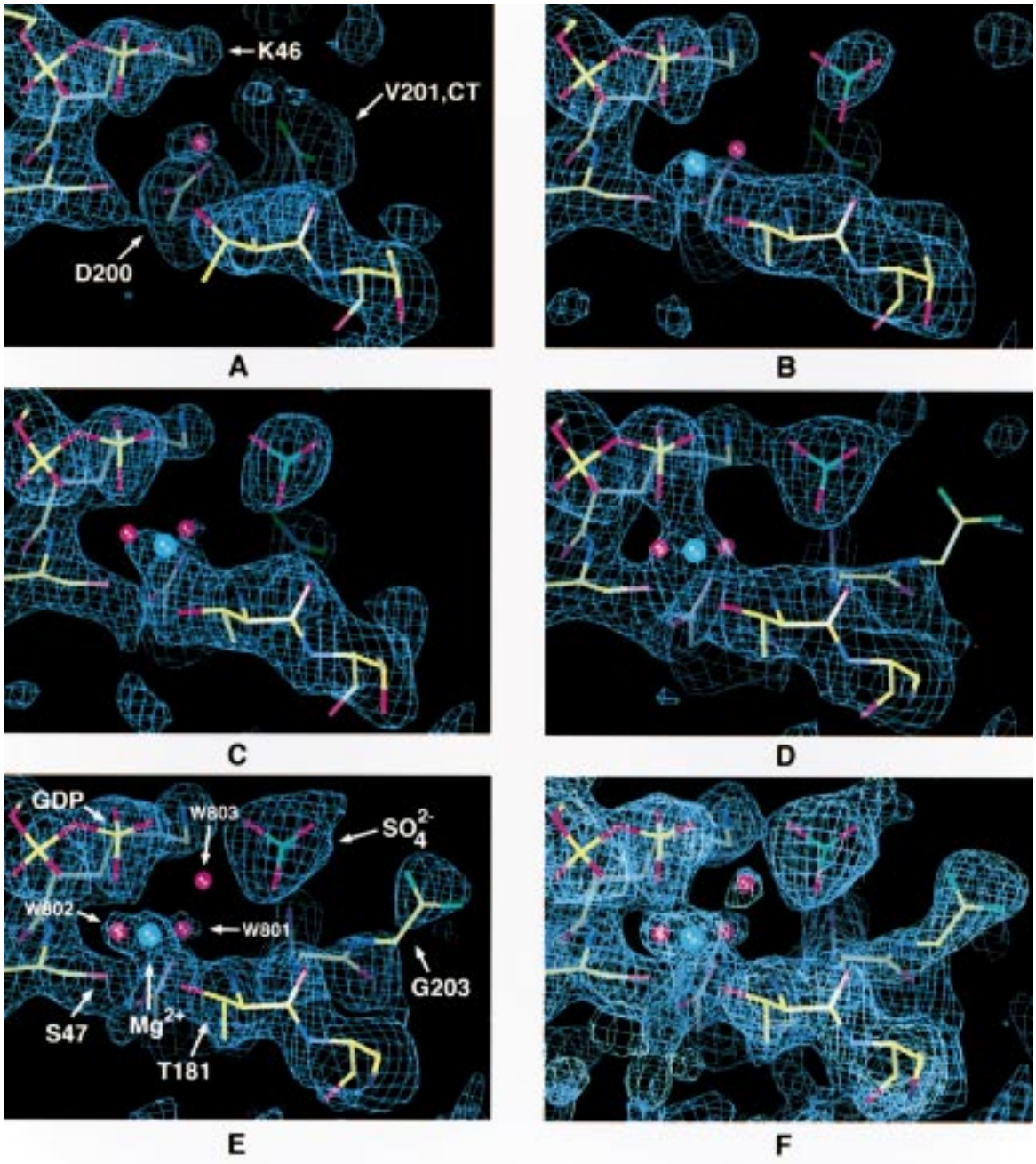

FIGURE 2: Simulated annealing omit maps about the Mg^{2+} binding site of the $G_{i\alpha1}$·GDP and $G_{i\alpha1}$·GDP·Mg^{2+} structures. Blue contours correspond to $F_o - F_c$ density in which GDP, SO_4^{2-}, Mg^{2+}, and protein and water molecules within 3 Å were omitted from the simulated annealing refinement and the phasing model. Green contours in panel F correspond to $2F_o - F_c$ electron density generated using the entire final refined model. GDP, Mg^{2+}, SO_4^{2-}, and selected waters and protein residues are labeled in panels A and E. The atoms at the carboxyl end of V201 (0, 5, and 10 mM Mg^{2+}) and G203 (100 and 200 mM Mg^{2+}) are colored green; the residues following V201 or G203 are disordered; thus, these atoms cannot be assigned as either oxygen or nitrogen. Map contour levels and resolution are as follows: (A) 0 mM Mg^{2+} (2.3 Å, 2.0σ), (B) 5 mM Mg^{2+} (2.6 Å, 2.0σ), (C) 10 mM Mg^{2+} (2.2 Å, 2.0σ), (D) 100 mM Mg^{2+} (2.6 Å, 2.0σ), (E) 200 mM Mg^{2+} (2.2 Å, 2.0σ), and (F) 200 mM Mg^{2+} (2.2 Å, 1.5σ for both the $2F_o - F_c$ and $F_o - F_c$ maps).

47 is part of the diphosphate binding loop or P-loop, a highly conserved sequence motif [^{40}GXXXXGK(S/T)] present in all G proteins. The two axial ligands are water molecules (waters 801−802), one of which (water 801) is also found in the Mg^{2+}-free structure. The latter forms a hydrogen bond with the side chain of Asp 200, which is part of a conserved sequence motif, ^{200}DXXG, found in all regulatory GTP binding proteins (*5*), and forms the amino-terminal segment of switch II. Aspartate 200 serves to connect the Mg^{2+} site to switch II via axial water 801 that is bound to the Mg^{2+}. In the $G_{i\alpha1}$·GDP·Mg^{2+} structures, Asp 200 moves up to 1.0 Å toward the G domain and Ser 47, and assumes a conformation and hydrogen binding scheme that is equivalent to that observed in the $G_{i\alpha1}$·GTPγS·Mg^{2+} structure (Figure 5). In particular, the distance between the side chain hydroxyl group of Ser 47 and a carboxylate oxygen of Asp 200 is reduced from 3.8 to 3.0 Å. The Mg^{2+}/ligand bond distances are indicated in Figure 5a. Excluding the 2.7 Å separation between Mg^{2+} and the low occupancy equatorial water 803, these average 2.2 Å and are similar to those observed in the $G_{i\alpha1}$·GTPγS·Mg^{2+} structure and other Mg^{2+}−protein complexes. The longer bond distance ob-

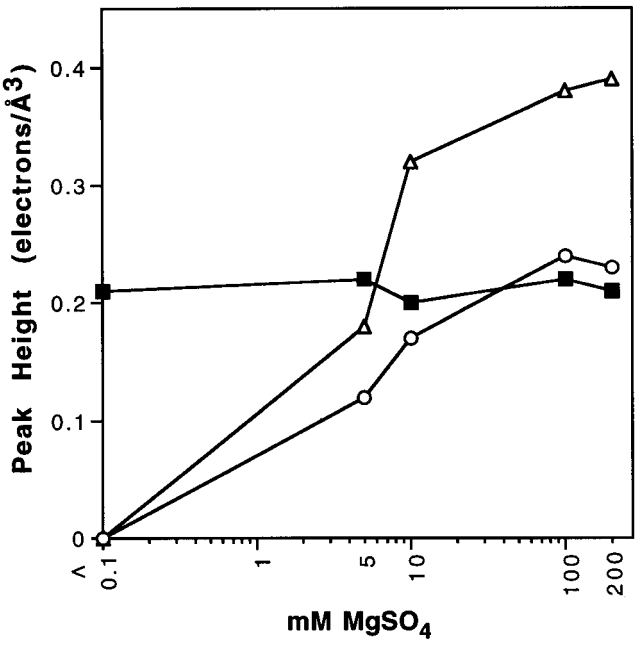

FIGURE 3: Maximum peak heights at the positions of the Mg^{2+} (circles), the active site SO_4^{2-} (triangles), and alanine 41 (filled squares) observed in 15−2.6 Å $F_o - F_c$ omit maps of the Mg^{2+}-free and Mg^{2+}-bound $G_{i\alpha1}$·GDP structures plotted vs the [$MgSO_4$]. Mg^{2+} and the active site SO_4^{2-} were omitted from the calculated phases and amplitudes. Ala 41 was also omitted as a control (see Experimental Procedures).

served between Mg^{2+} and equatorial water 803 indicates that this interaction is weaker than those with the other ligands, as is also indicated by the weak electron density observed for this water ligand. The second sphere ligands of the Mg^{2+} coordination sphere are identical to those observed in the $G_{i\alpha1}$·GTPγS·Mg^{2+} structure (Figure 5).

Mg^{2+}-Induced Changes in the Conformation of Switch I. Mg^{2+} binding alters switch I, leading it to a conformation similar to that observed in the active $G_{i\alpha1}$·GTPγS·Mg^{2+} complex. In concert with increased occupancy of the Mg^{2+} binding site, residues 180−182 of switch I progressively move toward the Mg^{2+} site (Figure 6). This ensemble of conformations shows that switch I exhibits plasticity with respect to Mg^{2+} binding. In the $G_{i\alpha1}$·GDP·$Mg^{2+}{}_{200mM}$ structure, the Cα atoms of Lys 180 and Thr 181 have moved, respectively, 1.7 and 1.2 Å away from their positions in the $G_{i\alpha1}$·GDP structure and assume a conformation similar to that observed in the active $G_{i\alpha1}$·GTPγS·Mg^{2+} structure (Figure 6). This movement allows the hydroxyl group of Thr 181 to coordinate the Mg^{2+}. When the G domains of the Mg^{2+}-free $G_{i\alpha1}$·GDP and $G_{i\alpha1}$·GTPγS·Mg^{2+} structures are superimposed, the RMS difference between the Cα atoms of switch I residues 180−182 is 2.1 Å. A similar superposition between the $G_{i\alpha1}$·GDP·$Mg^{2+}{}_{200mM}$ and $G_{i\alpha1}$·GTPγS·Mg^{2+} structures gives an RMS difference of 1.0 Å. If only the α- and β-phosphate groups and the Mg^{2+} of the latter two structures are superimposed, the RMS difference between residues 180−182 falls to 0.54 Å. Therefore, the position of switch I relative to the γ-phosphate and Mg^{2+} sites is nearly the same in the GDP·Mg^{2+}- and GTPγS·Mg^{2+}-bound conformations. The interaction between the hydroxyl group of Thr 181 and Mg^{2+} appears to cause the changes in the conformation of switch I. In the $G_{i\alpha1}$·GDP structure, no electron density is observed for the side chain of Lys 180, indicating that it is disordered. The main chain of this residue is oriented such that its side chain would be directed out of the active site. However, the side chain of Lys 180 is observed as weak density in the $G_{i\alpha1}$·GDP·$Mg^{2+}{}_{100mM}$ and $Mg^{2+}{}_{200mM}$ structures, and it is directed into the active site where it interacts with an SO_4^{2-} ligand as discussed below.

In the $G_{i\alpha1}$·GTPγS·Mg^{2+} structure, the carbonyl oxygen of Thr 181 is hydrogen bonded to a well ordered water which, in $G_{i\alpha1}$ and other G protein structures, is positioned for nucleophilic attack upon the γ-phosphate of GTP (*12*, *20*, *22*, *52*−*54*). Although Thr 181 is in the correct

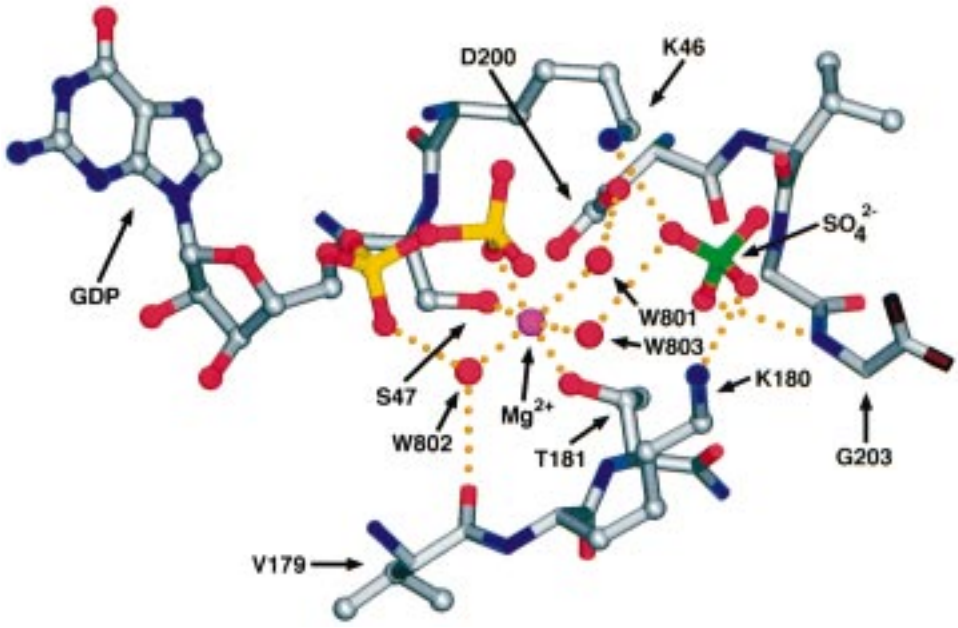

FIGURE 4: Mg^{2+} and SO_4^{2-} binding sites within the 200 mM Mg^{2+} $G_{i\alpha1}$·GDP·Mg^{2+}·SO_4^{2-} complex showing significant residues, ligands, and interactions. GDP, Mg^{2+}, SO_4^{2-}, waters, and key protein residues are labeled. Hydrogen bonds are indicated as dashed lines. The atoms at the carboxyl end of G203 are colored black; the residues following G203 are disordered; thus, these atoms cannot be assigned as either oxygen or nitrogen. This figure and Figure 6 were rendered with the program SETOR (*62*).

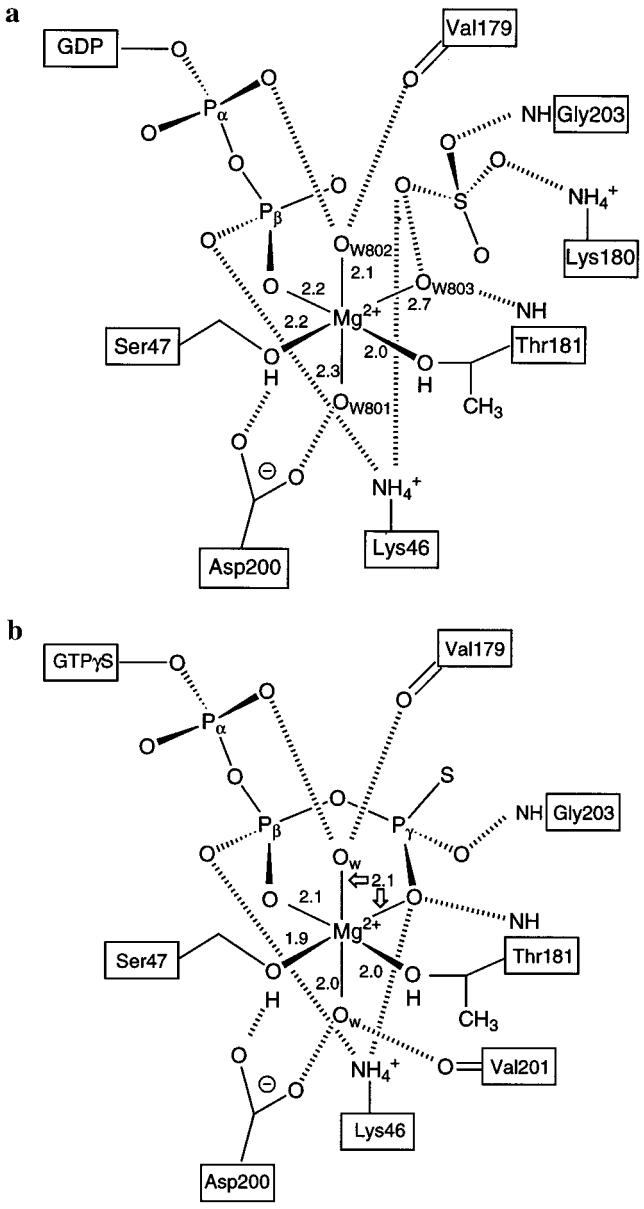

FIGURE 5: Schematic diagram of the octahedral Mg^{2+} binding site observed in the 200 mM Mg^{2+} $G_{i\alpha1}$·GDP·Mg^{2+}·SO_4^{2-} and $G_{i\alpha1}$·GTPγS·Mg^{2+} complexes showing the major interactions between protein residues and bound ligands. Distances between Mg^{2+} and its ligands are indicated in angstroms. Hydrogen bonding and salt bridge interactions are indicated as dashed lines. Formal charges on the phosphate and sulfate groups are not indicated. (a) $G_{i\alpha1}$·GDP·Mg^{2+}·SO_4^{2-}; (b) $G_{i\alpha1}$·GTPγS·Mg^{2+}.

conformation to bind this water molecule in the $G_{i\alpha1}$·GDP·Mg^{2+} structures, the water is not present, most likely because its other ligand, the γ-thiophosphate of GTPS, is absent. Mg^{2+} thus binds to the crystalline $G_{i\alpha1}$·GDP complex and, primarily by its direct interaction with the side chain hydroxyl group of Thr 181, stabilizes switch I and causes it to assume a conformation that is similar to that in the activated GTP-bound state.

Mg^{2+}-Induced Ordering of Switch II. Mg^{2+} binding leads to a partial ordering of switch II residues. In the Mg^{2+}-free $G_{i\alpha1}$·GDP structure, residues 202−217 of switch II are disordered and were not observed (*23*), whereas switch II in the $G_{i\alpha1}$·GTPγS·Mg^{2+} structure (*22*) is ordered and consists of a loop (residues 202−204) followed by a helix (residues 205−217) (Figure 1). Switch II is also ordered, although

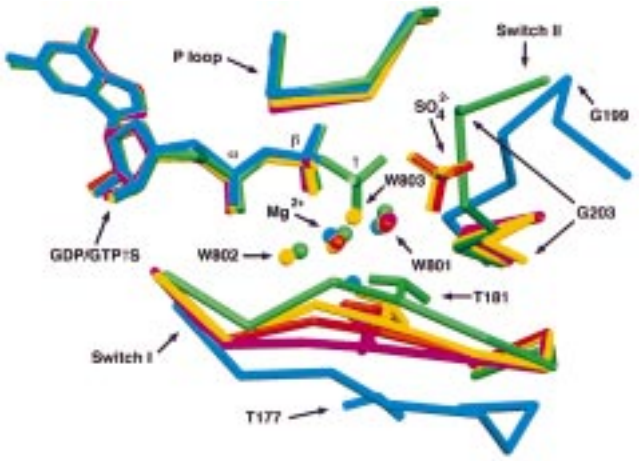

FIGURE 6: Mg^{2+}-induced structural transitions within switch I of the inactive $G_{i\alpha1}$·GDP complex and comparison with the structure of the active state of $G_{i\alpha1}$ ($G_{i\alpha1}$·GTPγS·Mg^{2+}) and the inactive state of transducin ($G_{t\alpha}$·GDP·Mg^{2+}). Selected main chain residues of switch I (177−185 $G_{i\alpha1}$, 173−181 $G_{t\alpha}$), switch II (199−201 $G_{i\alpha1}$·GDP and $G_{i\alpha1}$·GDP·$Mg^{2+}{}_{5mM}$, 199−203 $G_{i\alpha1}$·GDP·$Mg^{2+}{}_{200mM}$, 199−205 $G_{i\alpha1}$·GTPγS·Mg^{2+}, 195−201 $G_{t\alpha}$·GDP·Mg^{2}), and the P-loop (40−44 $G_{i\alpha1}$, 36−40 $G_{t\alpha}$) are shown as Cα traces; other features as labeled. The $G_{i\alpha1}$·GDP·Mg^{2+} and $G_{t\alpha}$·GDP·Mg^{2+} structures have been superimposed onto the G domain (residues 34−62, 177−343) of $G_{i\alpha1}$·GTPγS·Mg^{2+}: $G_{i\alpha1}$·GDP (magenta), $G_{i\alpha1}$·GDP·$Mg^{2+}{}_{5mM}$ (orange), $G_{i\alpha1}$·GDP·$Mg^{2+}{}_{200mM}$ (yellow), $G_{i\alpha1}$·GTPγS·Mg^{2+} (green), and $G_{t\alpha}$·GDP·$Mg^{2+}{}_{200mM}$ (blue). Views of the $G_{i\alpha1}$·GDP·$Mg^{2+}{}_{10mM}$ and $G_{i\alpha1}$·GDP·$Mg^{2+}{}_{100mM}$ structures are omitted for clarity.

with a different conformation, in the GDP·PO_4^{2-}-bound structures of the G203A (*38*) and S42V (*39*) mutants of $G_{i\alpha1}$. Likewise switch III, which is stabilized by contacts with switch II, is ordered in the structure of $G_{i\alpha1}$·GTPγS·Mg^{2+} but is disordered in the $G_{i\alpha1}$·GDP complex. In $G_{i\alpha1}$·GDP·$Mg^{2+}{}_{100mM}$ and $G_{i\alpha1}$·GDP·$Mg^{2+}{}_{200mM}$, continuous density for switch II residues 201−203 (VGG, part of the conserved ^{200}DXXG sequence) is observed, and disconnected density can be seen throughout the region that is occupied by the switch II helix in $G_{i\alpha1}$·GTPγS·Mg^{2+} (Figure 2E,F). As noted above, Asp 200 assumes the conformation and participates in the same interactions observed in the $G_{i\alpha1}$·GTPγS·Mg^{2+} structure. However, the conformation of residues 201−203 (Figure 4) differs from that observed in either the $G_{i\alpha1}$·GTPγS·Mg^{2+} structure or the GDP·PO_4^{2-}-bound structures of the G203A and S42V mutants of $G_{i\alpha1}$. Hence, Mg^{2+} binding promotes the active conformation of Asp 200 and an ordered conformation of certain switch II residues, but does not alone completely stabilize switch II or induce stability in switch III. Mg^{2+} may partially stabilize switch II by anchoring its amino terminus via the Mg^{2+}·H_2O·Asp^{200} interaction previously described. As noted under Experimental Procedures, crystals could not be grown de novo from solutions containing 100 or 200 mM Mg^{2+}. When the protein is saturated with Mg^{2+}, it may assume a solution conformation that differs from that observed in the Mg^{2+}-titrated crystals, in which switch II is more completely ordered. Inhibition of de novo crystallization by 100 and 200 mM Mg^{2+} may also be caused by the Mg^{2+}-induced movement of switch I toward the Mg^{2+} binding site, which partially breaks crystal lattice contacts between switch I and a neighboring molecule.

Mg^{2+}-Induced Recruitment of SO_4^{2-} to the Catalytic Site. Mg^{2+} binding causes an SO_4^{2-} molecule from the solvent to bind at the active site. Discrete electron density appears in a region of the active site of the $G_{i\alpha1}$·GDP·Mg^{2+} complexes that is unoccupied in the $G_{i\alpha1}$·GDP complex and is near, but not identical to, the position occupied by the γ-phosphate group in the $G_{i\alpha1}$·GTPγS·Mg^{2+} complex and the monophosphate in the structures of the G203A and S42V mutants of $G_{i\alpha1}$ bound to GDP·PO_4^{2-} (Figure 2). Based on its magnitude, shape, and proximity to protein side chains, this density was modeled as a sulfate ion derived from the 2.0 M Li_2SO_4 crystal stabilization media. The refined *B*-factors are consistent with this assignment. The occupancy of the SO_4^{2-} site increases as a function of the concentration of $MgSO_4$ in the soaking solution, and parallels the occupancy of the Mg^{2+} binding site (Figure 3), indicating that Mg^{2+} promotes SO_4^{2-} binding. However, Mg^{2+} and SO_4^{2-} do not directly contact each other; rather SO_4^{2-} interacts with several other components of the active site (Figures 4 and 5a). The sulfate is bound by interactions with the side chain of Lys 46 and the backbone amide of Gly 203. The SO_4^{2-} ion also interacts with water 803, the ligand that replaces the γ-phosphate oxygen in the equatorial plane of the Mg^{2+} coordination sphere. This latter interaction may be partially responsible for the Mg^{2+}-induced binding of sulfate to the active site. However, as noted, electron density for this water is weak and is only apparent in the $G_{i\alpha1}$·GDP·$Mg^{2+}{}_{200mM}$ structure. Hence, other Mg^{2+}-induced interactions may be important in binding the SO_4^{2-}. Mg^{2+} may further support SO_4^{2-} binding by stabilizing Gly 203 and the amino terminus of switch II via the hydrogen bond between one of its ligands, water 801, and Asp 200. Density for the side chain of Lys 180 is absent in the $G_{i\alpha1}$·GDP structure, but weak density appears in the $G_{i\alpha1}$·GDP·Mg^{2+} series. In the $G_{i\alpha1}$·GDP·$Mg^{2+}{}_{200mM}$ structure, side chain density for this residue is present except for the terminal amino group, and its conformation indicates that it contacts an oxygen of the active site SO_4^{2-}. This interaction may provide additional binding energy for SO_4^{2-}.

DISCUSSION

We have determined the structure of $G_{i\alpha1}$·GDP complexed with Mg^{2+} for several reasons. First, we wished to determine whether Mg^{2+} binds to crystalline $G_{i\alpha1}$·GDP. Although the $G_{i\alpha1}$·GDP structure was initially solved in the absence of Mg^{2+}, the presence of Mg^{2+} bound to the GDP·Mg^{2+}-bound complex of the homologous protein $G_{t\alpha}$ suggested that Mg^{2+} would bind to $G_{i\alpha1}$·GDP also. Second, we wished to determine if addition of Mg^{2+} to $G_{i\alpha1}$·GDP would induce order in the disordered switch II and III regions, as these regions are ordered in $G_{t\alpha}$·GDP·Mg^{2+}. Third, we sought to determine the mode of Mg^{2+} binding, and the nature of any other conformational changes that may occur relative to the Mg^{2+}-free $G_{i\alpha1}$·GDP structure. Mg^{2+}-induced conformational changes could represent events that occur during activation of $G_{i\alpha1}$ and release from heterotrimer, or changes within the active site during release of product. Our results indicate that crystalline $G_{i\alpha1}$·GDP, like $G_{t\alpha}$·GDP and other G proteins, does bind Mg^{2+}. However, although the location of the Mg^{2+} binding site is the same in all of these proteins, the identities of the metal ligands and conformations of the adjacent switch regions differ.

Binding of Mg^{2+} to crystalline $G_{i\alpha1}$·GDP does not induce a conformation of switch I similar to that observed in $G_{t\alpha}$·GDP·Mg^{2+} or induce extensive order in the disordered regions, switch II and III, which are well-ordered in $G_{t\alpha}$·GDP·Mg^{2+}. Therefore, the differences between the switch regions of $G_{t\alpha}$·GDP·Mg^{2+} and $G_{i\alpha1}$·GDP/$G_{i\alpha1}$·GDP·Mg^{2+} cannot be attributed to the presence or absence of Mg^{2+}, but rather may result from other factors, such as different crystal packing schemes. Switch I of $G_{i\alpha1}$·GDP lies near the N-terminal helix of a neighboring molecule, which prevents it from assuming a conformation similar to that observed in $G_{t\alpha}$·GDP·Mg^{2+}. Crystal packing interactions may push this switch toward the catalytic site. In contrast, crystals of $G_{t\alpha}$·GDP·Mg^{2+} were prepared with protein lacking the first 25 N-terminal residues, making such an interaction impossible. In crystals of $G_{t\alpha}$·GDP·Mg^{2+}, switch II makes extensive contacts with neighboring molecules that may serve to stabilize its structure. In contrast, the regions surrounding switch II in the $G_{i\alpha1}$·GDP/$G_{i\alpha1}$·GDP·Mg^{2+} structures are free from intermolecular contacts. Differences in the switch conformations exhibited by $G_{i\alpha1}$ and $G_{t\alpha}$·GDP may also be attributed to primary structure ($G_{i\alpha1}$ and $G_{t\alpha}$ share 65% sequence identity) and crystal growth and solvent systems ($G_{i\alpha1}$·GDP·Mg^{2+} crystals were grown and stabilized in high salt concentration systems at pH 7.0, and $G_{t\alpha}$·GDP·Mg^{2+} crystals were grown and stabilized in PEG 8000 at pH 6.0). In addition, the $G_{i\alpha1}$·GDP·Mg^{2+} structures contain SO_4^{2-} bound at the active site.

The inability of Mg^{2+} to induce order in switch II and III in the $G_{i\alpha1}$·GDP complex reinforces our hypothesis that these regions are disordered in the inactive state, and that this disorder is involved in dissociation from effector. The structure of a different G_α subunit, $G_{s\alpha}$, complexed with GTPS·Mg^{2+} and the catalytic domains of its effector, adenylyl cyclase, reveal that switch II interacts directly with the effector (*17*). The conformation of switch II in that complex is essentially identical to that of $G_{s\alpha}$·GTPS·Mg^{2+} alone (*52*) and of $G_{i\alpha1}$·GTPγS·Mg^{2+}. Given these similarities, it is likely that $G_{i\alpha1}$ also interacts with adenylyl cyclase via interactions with switch II. The loss of order of switch II following GTP hydrolysis would naturally lead to a loss of affinity for the effector and inactivation of the system.

The structure of $G_{i\alpha1}$·GDP·Mg^{2+} reported here displays a mode of Mg^{2+} binding which has not been previously observed in a G protein/GDP-bound complex. The Mg^{2+} binding mode is essentially identical to that observed in the active $G_{i\alpha1}$·GTPγS·Mg^{2+} structure, with the necessary difference that a water molecule replaces the absent γ-phosphate oxygen ligand. The conserved Thr residue of switch I binds to the Mg^{2+} as in the activated state. This is in contrast to the mode of Mg^{2+} binding observed in the structures of nonheterotrimeric G proteins such as Ras (*11*), Ran (*55*), Arf (*56*), Rap2A (*57*), and EF-TU (*58*) and the heterotrimeric G protein α subunit $G_{t\alpha}$. In these structures, the mode of Mg^{2+} binding differs between the GDP and GTP or GTP analogue bound states, and the conserved Thr of switch I participates in Mg^{2+} ligation in the active GTP-bound state only.

Many of the latter G proteins may require Mg^{2+} in order to bind GDP with high affinity, and consequently bind Mg^{2+} in both the active and inactive states at physiological [Mg^{2+}]. The transition from the active to the inactive state in these

proteins is thus driven entirely by loss of the γ-phosphate upon GTP hydrolysis. In contrast, most G_α subunits do not require Mg^{2+} in order to bind GDP or to form complexes with $G_{\beta\gamma}$. It has been proposed that the helical domains of G_α subunits promote nucleotide binding (*20*), thus eliminating the need for Mg^{2+} binding in order to prevent unwarranted nucleotide exchange and activation in G_α·GDP complexes.

The weak affinity of $G_{i\alpha1}$·GDP for Mg^{2+} at physiological [Mg^{2+}] implies that the $G_{i\alpha1}$·GDP·Mg^{2+} complex (and perhaps that of other similar complexes observed crystallographically at high [Mg^{2+}]) does not represent a stable physiological species. Rather, the similarity of the Mg^{2+} ligation sphere to that of the active $G_{i\alpha1}$·GTPγS·Mg^{2+} complex implies that we have forced the $G_{i\alpha1}$·GDP·Mg^{2+} complex into a state that may represent Mg^{2+}-dependent features of the active GTP·Mg^{2+}-bound state and the unstable complex of $G_{i\alpha1}$, GDP, and P_i. Further, this structure may exhibit features of a conformational state that lies on the pathway leading to Mg^{2+} and P_i release, and loss of effector binding.

The conformational change induced by the exchange of GDP for GTP·Mg^{2+} is in part due to the synergistic effects of Mg^{2+}. In vitro studies show that addition of Mg^{2+} to G_α·GTP causes an increase in tryptophan fluorescence intensity (*33*, *34*) and resistance to proteolysis by trypsin (*35*, *36*) at a site within switch II. The structures described here, although formed with GDP, provide some insight into the mechanism by which Mg^{2+} contributes to these conformational changes. As Mg^{2+} is added to crystals of the $G_{i\alpha1}$·GDP complex, switch I progressively assumes a conformation similar to that observed in the active $G_{i\alpha1}$·GTPγS·Mg^{2+} complex, even as switch II remains largely disordered. Hence, switch I activation is dependent primarily on Mg^{2+} binding and does not require that switch II be in its active conformation. The γ-phosphate would serve to activate switch I indirectly by recruiting Mg^{2+}. The Mg^{2+}-stabilized conformation of switch I may contribute to $G_{i\alpha1}$ activity in several ways. First, the movement of the switch toward the Mg^{2+} site would be expected to disrupt interactions between $G_{i\alpha1}$ and $G_{\beta\gamma}$ in the heterotrimer, thus contributing to dissociation of $G_{i\alpha1}$·GTP·Mg^{2+} from the complex (*59*). Second, the side chain of Thr 181 coordinates Mg^{2+}, and the main chain carbonyl oxygen of this residue reorients to occupy a position identical to that observed in the $G_{i\alpha1}$·GTPγS·Mg^{2+} complex, where it binds a water molecule that ultimately mounts a nucleophilic attack on the phosphate of GTP.

Addition of Mg^{2+} to the $G_{i\alpha1}$·GDP crystals also causes the conserved Asp 200 of switch II, which is a second sphere ligand of Mg^{2+}, to assume the conformation and participate in interactions that are observed in the $G_{i\alpha1}$·GTPγS·Mg^{2+} structure. These interactions may partially stabilize switch II, leading to the ordered conformation of switch II residues 202−203, but do not lead to full stabilization of switch II, which presumably requires the γ-phosphate of GTP for full stability in the active state.

An unexpected result of the Mg^{2+} titration experiment is the discovery that an SO_4^{2-} occupies the active site in proportion to the concentration of Mg^{2+} in the crystals. Sulfate appears to induce residues 201−203 of switch II to adopt an ordered conformation and partially stabilizes the remainder of switch II as indicated by the presence of scattered electron density. SO_4^{2-} and Mg^{2+} may bind synergistically, through their mutual interaction with the water molecule that substitutes for the oxygen of the γ-phosphate in GTP. Sulfate appears to order residues 201−203 of switch II by forming a hydrogen bond with the amide group of Gly 203, thereby inducing partial order in the remainder of switch II. Magnesium ions might stabilize residues 201−203 indirectly by anchoring the carboxylate of the neighboring residue Asp 200 via water 801 (Figure 4). This set of interactions may also contribute to Mg^{2+}-induced binding of SO_4^{2-}. However, the SO_4^{2-} site is well occupied in the 10 mM Mg^{2+} structure whereas extensive density in the 201−203 region appears only in crystals containing 100 and 200 mM Mg^{2+}. Hence, the SO_4^{2-}, and, by analogy, phosphate, may bind even if the amino terminus of switch II is largely disordered. Nevertheless, the Mg^{2+}- and SO_4^{2-}-induced conformational changes in switch I and II are no doubt synergistic.

With SO_4^{2-} serving as an analogue of PO_4^{2-}, the $G_{i\alpha1}$·GDP·Mg^{2+}·SO_4^{2-} series of structures, formed in the presence of increasing magnesium concentrations, may mimic the conformational changes that occur upon release of phosphate and Mg^{2+} from the quaternary product complex after GTP hydrolysis. Although the body of the switch II helix is disordered, its amino terminus adopts an ordered conformation. However, the switch is displaced outward from the active site in order to accommodate the quaternary product complex of GDP, Mg^{2+}, and SO_4^{2-} (Figure 6). As with the γ-phosphate of the GTPγS complex, Gly 203 forms a hydrogen bond with SO_4^{2-}. We therefore infer that cleavage of the $\beta-\gamma$ bond of GTP is accompanied by a conformational change in switch II that creates a binding site for the product phosphate. Formation of the GDP·P_i complex in the G203A and S42V mutants of $G_{i\alpha1}$ is also accompanied by a substantial rearrangement of switch II, but the switch is kinked in the middle and fully ordered (*38*, *39*). The phosphate ion in those complexes is also hydrogen bonded to Gly 203, but, unlike the structures described here, is directly hydrogen bonded to Thr 181 in switch I. The crystals of the $G_{i\alpha1}$ mutants were prepared at pH <6 and, perhaps as a consequence, contain no Mg^{2+} in the active site. Therefore, it is possible that the quaternary GDP·Mg^{2+}·SO_4^{2-} complexes described here are better mimics of the quaternary product complex formed at physiological pH. Nevertheless, SO_4^{2-} is an imperfect analogue of the monoprotonated P_i, and hence its interaction with the active site of $G_{i\alpha1}$ may differ.

From the series of structures presented here, we can infer that loss of PO_4^{2-} and Mg^{2+} from the active site is concerted. In vivo, this event leads to dissociation of $G_{i\alpha1}$ from its effector. Upon GTP hydrolysis, PO_4^{2-} moves away from the active site while maintaining hydrogen bond contact with G203 of switch II. Complete release of Mg^{2+} and PO_4^{2-} leads to total destabilization of the switch, and corresponding 10-fold reduction in affinity for adenylyl cyclase.

ACKNOWLEDGMENT

We thank Ward Coates, Todd Harrell, Mark Mixon, Bryan Sutton, John Tesmer, Mark Wall, Tsan Xiao, and the staff

at the Cornell High Energy Synchrotron Source (CHESS) for assistance with data collection.

REFERENCES

1. Gilman, A. G. (1987) *Annu. Rev. Biochem. 56*, 615−649.
2. Kaziro, Y., Itoh, H., Kozasa, T., Nakafuku, M., and Satoh, T. (1991) *Annu. Rev. Biochem. 60*, 349−400.
3. Ross, E. M. (1996) *Recent Prog. Horm. Res. 50*, 207−221.
4. Berman, D. M., and Gilman, A. G. (1998) *J. Biol. Chem. 273*, 1269−1272.
5. Bourne, H. R., Sanders, D. A., and McCormick, F. (1991) *Nature 349*, 117−127.
6. Bourne, H. R., Sanders, D. A., and McCormick, F. (1990) *Nature 348*, 125−132.
7. Cotecchia, S., Kobilka, B. K., Daniel, K. W., Nolan, R. D., Lapetina, E. Y., Caron, M. G., Lefkowitz, R. J., and Regan, J. W. (1990) *J. Biol. Chem. 265*, 63−69.
8. Migeon, J. C., Thomas, S. L., and Nathanson, N. M. (1995) *J. Biol. Chem. 270*, 16070−16074.
9. Taussig, R., Iñiguez-Lluhi, J. A., and Gilman, A. G. (1993) *Science 261*, 218−221.
10. Taussig, R., Tang, W.-J., Hepler, J. R., and Gilman, A. G. (1994) *J. Biol. Chem. 269*, 6093−6100.
11. Tong, L., De Vos, A. M., Milburn, M. V., and Kim, S.-H. (1991) *J. Mol. Biol. 217*, 503−516.
12. Pai, E. F., Krengel, U., Petsko, G. A., Goody, R. S., Kabsch, W., and Wittinghofer, A. (1990) *EMBO J. 9*, 2351−2359.
13. Milburn, M. V., Tong, L., deVos, A. M., Brünger, A., Yamaizumi, Z., Nishimura, S., and Kim, S.-H. (1990) *Science 247*, 939−945.
14. Kjeldgaard, M., Nyborg, J., and Clark, B. F. C. (1996) *FASEB J. 10*, 1347−1368.
15. Sprang, S. R. (1997) *Annu. Rev. Biochem. 66*, 639−678.
16. Nassar, N., Horn, G., Herrmann, C., Scherer, A., McCormick, F., and Wittinghofer, A. (1995) *Nature 375*, 554−560.
17. Tesmer, J. J. G., Sunahara, R. K., Gilman, A. G., and Sprang, S. R. (1997) *Science 278*, 1907−1916.
18. Wall, M. A., Coleman, D. E., Lee, E., Iñiguez-Lluhi, J. A., Posner, B. A., Gilman, A. G., and Sprang, S. R. (1995) *Cell 80*, 1047−1058.
19. Lambright, D. G., Sondek, J., Bohm, A., Skiba, N. P., Hamm, H., and Sigler, P. B. (1996) *Nature 379*, 311−319.
20. Noel, J. P., Hamm, H. E., and Sigler, P. B. (1993) *Nature 366*, 654−663.
21. Lambright, D. G., Noel, J. P., Hamm, H. E., and Sigler, P. B. (1994) *Nature 369*, 621−628.
22. Coleman, D. E., Berghuis, A. M., Lee, E., Linder, M. E., Gilman, A. G., and Sprang, S. R. (1994) *Science 265*, 1405−1412.
23. Mixon, M. B., Lee, E., Coleman, D. E., Berghuis, A. M., Gilman, A. G., and Sprang, S. R. (1995) *Science 270*, 954−960.
24. Ivell, R., Sander, G., and Parmeggiani, A. (1981) *Biochemistry 20*, 6852−6859.
25. Arai, K.-I., Kawakita, M., and Kaziro, Y. (1972) *J. Biol. Chem. 247*, 7029−7037.
26. Hall, A., and Self, A. J. (1986) *J. Biol. Chem. 261*, 10963−10965.
27. Pan, J. Y., Sanford, J. C., and Wessling-Resnick, M. (1996) *J. Biol. Chem. 271*, 1322−1328.
28. John, J., Rensland, H., Schlichting, I., Vetter, I., Borasio, G. D., Goody, R. S., and Wittinghofer, A. (1993) *J. Biol. Chem. 268*, 923−929.
29. Kawashima, T., Berthet-Colominas, C., Wulff, M., Cusack, S., and Leberman, R. (1996) *Nature 379*, 511−518.
30. Wang, Y., Jiang, Y., Meyering-Voss, M., Sprinzl, M., and Sigler, P. B. (1997) *Nat. Struct. Biol. 4*, 650−656.
31. Higashijima, T., Ferguson, K. M., Sternweis, P. C., Smigel, M. D., and Gilman, A. G. (1987) *J. Biol. Chem. 262*, 762−766.
32. al-Karadaghi, S., AEvarsson, A., Garber, A., Zheltonosova, J., and Liljas, A. (1996) *Structure 4*, 555−565.
33. Higashijima, T., Ferguson, K. M., Sternweis, P. C., Ross, E. M., Smigel, M. D., and Gilman, A. G. (1987) *J. Biol. Chem. 262*, 752−756.
34. Phillips, W. J., and Cerione, R. A. (1986) *J. Biol. Chem. 263*, 15498−15505.
35. Fung, B. K.-K., and Nash, C. R. (1983) *J. Biol. Chem. 258*, 10503−10510.
36. Hurley, J. B., Simon, M. I., Teplow, D. B., Robishaw, J. D., and Gilman, A. G. (1984) *Science 226*, 860−862.
37. Lee, E., Taussig, R., and Gilman, A. G. (1992) *J. Biol. Chem. 267*, 1212−1218.
38. Berghuis, A. M., Lee, E., Raw, A. S., Gilman, A. G., and Sprang, S. R. (1996) *Structure 4*, 1277−1290.
39. Raw, A. S., Coleman, D. E., Gilman, A. G., and Sprang, S. R. (1997) *Biochemistry 36*, 15660−15669.
40. Lee, E., Linder, M. E., and Gilman, A. G. (1994) *Methods Enzymol. 237*, 146−164.
41. Coleman, D. E., Lee, E., Mixon, M. B., Linder, M. E., Berghuis, A., Gilman, A. G., and Sprang, S. R. (1994) *J. Mol. Biol. 238*, 630−634.
42. Otwinowski, Z., and Minor, W. (1997) *Methods Enzymol. 276*, 307−326.
43. Collaborative computing Project, Number 4 (1994) *Acta Crystallogr. D50*, 760−763.
44. Brünger, A. T. (1992) in *XPLOR Version 3.1: A system for X-ray crystallography and NMR*, Yale University Press, New Haven, CT.
45. Read, R. J. (1986) *Acta Crystallogr. A42*, 140−149.
46. Hodel, A., Kim, S.-H., and Brünger, A. T. (1992) *Acta Crystallogr. A48*, 851−858.
47. Jones, T. A., and Kjeldgaard, M. O. (1993) in *O Version 5.9*, Uppsala University, Uppsala.
48. Jones, T. A., Zou, J.-Y., Cowan, S. W., and Kjeldgaard, M. O. (1991) *Acta Crystallogr. A47*, 110−119.
49. Jiang, J. S., and Brünger, A. T. (1994) *J. Mol. Biol. 243*, 100−115.
50. Brünger, A. T. (1992) *Nature 355*, 472−475.
51. Laskowski, R. A., MacArthur, M. W., Moss, D. S., and Thornton, J. M. (1993) *J. Appl. Crystallogr. 26*, 283−291.
52. Sunahara, R. K., Tesmer, J. J. G., Gilman, A. G., and Sprang, S. R. (1997) *Science 278*, 1943−1947.
53. Berchtold, H., Reshetnikova, L., Reiser, C. O. A., Schirmer, N. K., Sprinzl, M., and Hilgenfeld, R. (1993) *Nature 365*, 126−132.
54. Hirshberg, M., Stockley, R. W., Dodson, G., and Webb, M. R. (1997) *Nat. Struct. Biol. 4*, 147−152.
55. Scheffzek, K., Klebe, C., Fritz-Wolf, K., Kabsch, W., and Wittinghofer, A. (1995) *Nature 374*, 378−381.
56. Greasley, S. E., Jhoti, H., Teahan, C., Solari, R., Fensome, A., Thomas, G. M. H., Cockcroft, S., and Bax, B. (1995) *Nat. Struct. Biol. 2*, 797−806.
57. Cherfils, J., Menetrey, J., Le Bras, G., Janoueix-Lerosey, I., de Gunzburg, J., Garel, J.-R., and Auzat, I. (1997) *EMBO J. 16*, 5582−5591.
58. Kjeldgaard, M., and Nyborg, J. (1992) *J. Mol. Biol. 223*, 721−742.
59. Wall, M. A., Posner, B. A., and Sprang, S. R. (1998) *Structure* (in press).
60. Kraulis, P. J. (1991) *J. Appl. Crystallogr. 24*, 946−950.
61. Bacon, D., and Anderson, W. F. (1988) *J. Mol. Graphics 6*, 219−220.
62. Evans, S. V. (1993) *J. Mol. Graphics 11*, 134−138.

BI9810306